Article:

Wolstenholme, JM, Smith, MW orcid.org/0000-0003-4361-9527, Baird, AJ orcid.org/0000-0001-8198-3229 et al. (1 more author) (2020) A new approach for measuring surface hydrological connectivity. Hydrological Processes, 34 (3). pp. 519-873. ISSN 0885-6087

https://doi.org/10.1002/hyp.13602

Authors:
Joshua M. Wolstenholme (Orcid ID: 0000-0001-9244-7210)

Mark W. Smith (Orcid ID: 0000-0003-4361-9527)

Andy J. Baird (Orcid ID: 0000-0001-8198-3229)

Thomas G. Sim (Orcid ID: 0000-0001-8604-9996)

A new approach for measuring surface hydrological connectivity

Running title: Measuring surface hydrological connectivity

Wolstenholme, J.M.[1,2]*, Smith, M.W.[1], Baird, A.J.[1] and Sim, T.G.[1]

[1] School of Geography, University of Leeds, Leeds, LS2 9JT, UK
[2] Energy and Environment Institute, University of Hull, Hull, HU6 7RX, UK

* Corresponding author: j.wolstenholme-2018@hull.ac.uk

Acknowledgements

The authors declare that there is no conflict of interest regarding the publication of this paper. The authors would also like to thank Tsz Long Lam for the use of UAV imagery and the School of Geography, University of Leeds for funding travel.

A new approach for measuring surface hydrological connectivity

Abstract

The development of surface hydrological connectivity is a key determinant of flood magnitude in drylands. Thresholds in runoff response may be reached when isolated runoff-generating areas connect with each other to form continuous links to river channels, enabling these areas to contribute to flood hydrographs. Such threshold behaviour explains observed nonlinearities and scale dependencies of dryland rainfall-runoff relationships and complicates attempts at flood prediction. However, field methods for measuring the propensity of a surface to transmit water downslope are lacking, and conventional techniques of infiltration measurement are often inappropriate for use on non-agricultural drylands. Here we argue for a reconceptualization of the dryland surface runoff process, suggesting that the downslope transfer of water should be considered alongside surface infiltration; i.e., there is a need for the 'aggregated' measurement of infiltration and overland flow hydraulics. Surface application of a set volume of water at a standardised rate generates runoff that travels downslope; the distance it travels downslope is determined by infiltration along the flow, integration of flow paths and flow resistance. We demonstrate the potential of such a combined measurement system coupled with Structure from Motion photogrammetry to identify surface controls on runoff generation and transfer on dryland hillslopes, with vegetation, slope, surface stone cover and surface roughness all having a significant effect. The measurement system has been used on slopes up to 37° compared to the flat surface typically required for infiltration methods. On average, the field workflow takes ~10-15 minutes, considerably quicker than rainfall simulation. A wider variety of surfaces can be sampled with relative ease, as the method is not restricted to stone and vegetation-free land. We argue that this aggregated measurement represents surface connectivity and dryland runoff response better than standard hydrological approaches, and can be applied on a much greater variety of dryland surfaces.

Keywords: infiltration; drylands; surface runoff; roughness; connectivity; flow pathways; flow resistance; Structure from Motion

1. Introduction

Drylands cover approximately 41% of the Earth's land surface (Middleton & Thomas, 1997) and are home to over 38% of the planet's population (Huang et al., 2017). Unlike more humid environments, the seasonal (or permanent) moisture deficit of drylands means that many river flows are ephemeral; when floods occur, they can be torrential and flashy. Modelling the development of such floods is challenging because large surface runoff generating areas may be initially isolated from the channel network by downslope infiltration (Ambroise, 2004). When surface hydrological connections between surface runoff source areas and river channels are eventually established, nonlinearities are introduced in rainfall-runoff relationships as source areas begin to contribute towards river discharge (Bracken & Croke, 2007; Smith, Bracken, & Cox, 2010; Wainwright & Bracken, 2011). A number of definitions of hydrological connectivity have emerged in the literature (see Ali & Roy, 2009); however, in a general sense, hydrological connectivity can be defined as, "the passage of water from one part of the landscape to another … expected to generate some catchment runoff response" (Bracken & Croke, 2007, p.1). Understanding how ground surface characteristics, infiltration and overland flow hydraulics influence surface hydrological connectivity in drylands is paramount to identifying areas vulnerable to erosion and flash flooding and informing targeted catchment management strategies.

Surface runoff generation in arid areas is extremely spatially variable and often controlled by localised convectional precipitation (Wolman & Gerson, 1978) superimposed on a patchwork of variable soil surface physical and chemical properties (Fitzjohn, Ternan, & Williams, 1998; Martínez-Mena, Albaladejo, & Castillo, 1998). Once the local surface runoff threshold has been satisfied by rainfall, water redistribution and downslope fluxes are dominated by overland flows that route water to the hillslope or catchment outlet. The degree to which isolated surface runoff generating areas are connected to the drainage network is a key determinant of flood magnitude; yet we know little about the dynamics of this connection process. Relationships have been observed between surface runoff and mapped flow lengths connecting source and outlet areas in drylands (Mayor, Bautista, Small, Dixon, & Bellot, 2008), but there have been few attempts to represent the connection process itself in a metric of connectivity (Heckmann et al., 2018). Downslope water fluxes via overland flows must overcome a combination of flow resistance and downslope transmission losses to reach an outlet (Mueller, Wainwright, & Parsons, 2007; Smith et al., 2010). While much has been done to improve our conceptualisation of this functional (or process-based) connectivity (Bracken et al., 2013; Kirkby, Bracken, & Reaney, 2002; Reaney, Bracken, & Kirkby, 2007; Reaney, Bracken, & Kirkby, 2014; Schreiner-McGraw &, Vivoni, 2019; Turnbull, Wainwright, & Brazier, 2008), we still know little about the real-world operation of the processes making and maintaining the connections.

Thus, we argue that the downslope surface transfer of water fluxes (functional or process-based connectivity) deserves much greater focus within our conceptual models of dryland hydrological response. Field campaigns should acquire data of such water fluxes to supplement the more conventional approach of identifying and mapping variability in local infiltration rates (structural connectivity). Simple measurement and modelling methods are required to represent these fluxes (Keestra et al., 2018). However, even infiltration in drylands remains poorly understood, because standard measurement techniques are often not suited to, or designed for, typical dryland surfaces. Around 65% of dryland areas are classified as rangeland (compared with 25% dedicated to agriculture; Safriel et al., 2005); however, existing infiltration measurement methods usually cannot be used on steep slopes, and slopes with stone or natural (or semi-natural) vegetation cover, without disturbing the soil.

The aim of this paper is to introduce a new field method that is well suited to dryland environments and can quantify the ability of a surface to develop and maintain surface hydrological connections. In doing so, we first highlight the shortcomings of both standard infiltration measurement methods and the characterisation of surface runoff when applied in a natural dryland setting (section 2). Second, we introduce a new conceptually simple and 'light-touch' field measurement method that is more suited to drylands and yields an aggregate measure of: (a) localised surface water losses via infiltration; and (b) the potential for surface hydrological connectivity development via overland flows (section 3). Third, we demonstrate the new field method in a dryland environment and use it to quantify the effects of soil surface properties on surface hydrological connectivity development (section 4).

2. Measuring infiltration and surface runoff in drylands

Infiltration is measured regularly in drylands throughout the world, predominantly on agricultural soils. Rainfall simulators are the most commonly used method (e.g. Arnau-Rosalen, Calvo-Cases, Boix-Fayos, Lavee, & Sarah, 2008; Bergkamp, Cerda, & Imeson, 1999; Dimanche, & Hoogmoed, 2002; Heilweil, Mckinney, Zhdanov, & Watt, 2007; Hikel et al., 2013; Pierson et al., 2010; Seeger, 2007; Simonneaux et al., 2015; Williams, Wuest, Schillinger, & Gollany, 2006;) and enable the indirect calculation of infiltration rates through the continuity equation by simultaneously measuring applied rainfall rates and observed surface runoff from a defined plot (Figure 1A). The time between rainfall and the start of ponding is also recorded to determine time until infiltration capacity is achieved.

Rainfall simulators can be adapted to a variety of plot sizes (from 0.25 m^2 to 20 m^2) to suit the needs of the user, so long as the chosen rainfall application method can effectively distribute water over the area. However, field applications are rarely >10 m^2 owing to increasing complexity and difficulties in transporting both the equipment and the substantial volumes of water needed for it (Williams et al., 2006). The popularity of rainfall simulators in drylands is well justified. This non-contact method disturbs only the periphery of the chosen plot and has the advantage of being applicable over a range of surface types (e.g. over low-stature vegetation, stone cover) while also replicating natural crust development from rainfall (Chen, Sela, Svoray, & Assouline, 2013). It allows surface runoff generation under natural conditions and, depending on plot size, incorporates a degree of local spatial variability in soil properties, allowing for downslope infiltration of surface runoff before reaching the plot outlet.

An additional advantage of rainfall simulators is that, unlike with other measurement techniques, surface runoff patterns can also be characterised, though a capture trough prevents surface flow over large areas. Surface influences on overland flow such as microtopography (e.g. Abrahams, Li, Krishnan, & Atkinson, 1998; Dunkerley, 2004) and vegetation (e.g. Abrahams, Parsons, & Wainwright, 1995; Mayor et al., 2008; Wainwright, Parsons, & Abrahams, 2000) have been quantified in this way. Recent rainfall experiments demonstrating that intermittent precipitation has a large influence on surface runoff generation (Dunkerley, 2018) have highlighted the complexities of dryland surface hydrology.

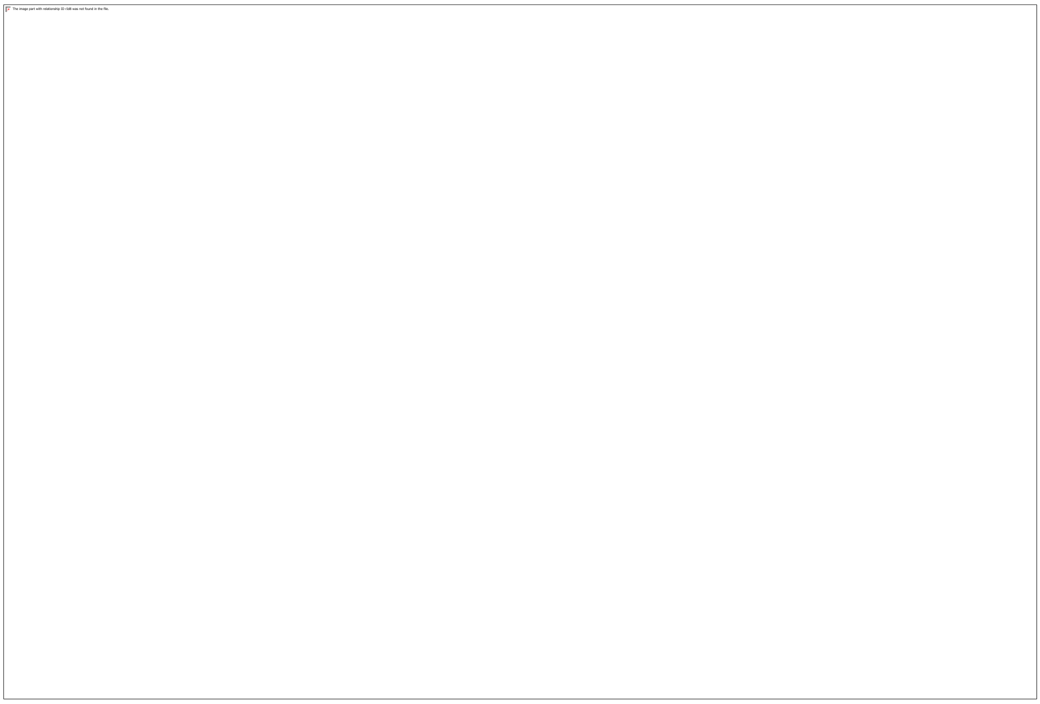

Figure 1. Infiltration methods commonly used in drylands. (A) rainfall simulator, (B) single-ring infiltrometer (adapted from Sanders, 1998), (C) double-ring infiltrometer (adapted from Sanders, 1998), (D) tension infiltrometer (adapted from Amoozegar and Wilson, 1999), (E) Minidisk tension infiltrometer (adapted from Decagon Devices, 2016).

The use of infiltrometers partly overcomes the logistical challenges of using rainfall simulators, allowing for greater replication of measurements, albeit at the expense of introducing a number of physical sources of measurement error (Reynolds, Elrick, Youngs, & Amoozegar, 2002). The most basic infiltrometer design, the single ring infiltrometer, is a cylinder composed of metal or plastic, ranging from 13-20 cm in diameter (Xu, Lewis, Liu, Albertson, & Kiely, 2012) which is inserted vertically ~6 cm into the ground (Figure 1B). Achieving this depth of insertion can be challenging on the majority of natural dryland surfaces with crusted, shallow and stony soils (Verbist et al., 2010). A sledgehammer is often required which breaks up the important surface crust layer formed from previous storms around the ring perimeter (Perrolf & Sandstrom, 1995). A level surface is also required to ensure a constant hydraulic head over the measurement area. Moreover, vegetation must be removed or trimmed to the base of the stems prior to measurement. Once the measurement begins, infiltration depth is recorded and timed and a near-constant head is maintained. Thus, a ponded infiltration rate is observed which may not represent natural water application rates and, owing to the lack of an impact crust, may overestimate storm infiltration rates (Chen et al., 2013), though gradual plugging of soil pores from deflocculated silts and clays may counteract this effect (Reynolds et al., 2002).

Moreover, the assumed vertical progression of the wetting front cannot be guaranteed (Sanders, 1998); lateral spreading may again lead to an overestimation of infiltration (Figure 1B). This final limitation is partially overcome by the use of a double ring infiltrometer, where a second outer ring is inserted deeper into the soil and the space between the rings is filled with water prior to the start of the test (Figure 1C) (Al-Awadhi, 2013; Guzha, 2004; Perrolf & Sandstrom, 1995; Verbist, Cornelis, Torfs, & Gabriels, 2013). The outer ring of water is designed to prevent lateral spreading from the inner ring; however, some initial lateral spreading of the outer ring before filling of the inner ring may cause underestimation of the initial infiltration rate. Both single and double ring infiltrometers sample only a small area; increasing the size of the inner ring incorporates greater local variability and, with diameters above 20 cm, has been shown to minimise the lateral spreading problem (Lai & Ren, 2007; Verbist et al., 2010; Wu & Pan, 1997), though greater volumes of water will be required for larger rings.

Tension infiltrometers permit the targeting of specific pore sizes to examine their contribution to infiltration. By gradually increasing the tension or negative pressure head of the water supply reservoir (Figure 1D), increasingly smaller pore sizes (starting from the largest) are excluded from conducting water into the soil (Brady & Weil, 2008), thereby permitting direct comparison of infiltration rates for different soil pore sizes (Kelishadi, Mosaddeghi, Hajabbasi, & Ayoubi, 2014; Verbist et al., 2013; Young, McDonald, Caldwell, Benner, & Meadows, 2004; Zhou, Hu, Cheng, Way, & Li, 2011). While tests can run for longer than ring infiltrometers, measurements can be automated to reduce the burden of field time and enable multiple simultaneous tests (Ankeny, Kaspar, & Horton, 1988). As with the ring infiltrometers, it is essential that vegetation is trimmed to surface height prior to starting a measurement, and any rough surfaces should be levelled to ensure a good hydraulic connection (Perroux & White, 1988). Clearly, this requirement limits the applicability of tension infiltrometers on the majority of natural surfaces that are sloping, and contain stones or vegetation. Thus, sampled surfaces are not representative of dryland conditions.

Tension infiltrometers are often large and bulky, but more-readily transportable versions, requiring a substantially lower volume of water (Li, Gonzalez, & Sole-Bennet, 2005; Smith, Cox, & Bracken, 2011) have been developed – e.g., Minidisk tension infiltrometers – and allow more rapid measurements. While each measurement samples only a very small area, the rapidity with which measurements can be taken enables local variability to be assessed through multiple distributed measurements. Also, the small size is well suited to drylands as small gaps between stones and vegetation can be measured, thereby permitting broader coverage of measurements. Certainly, for ease of use, practicality, time, cost and low water requirements, the Minidisk infiltrometer appears to be the preferred infiltration measuring method.

To summarise, there exists a trade-off between practicality and process representation when measuring infiltration in drylands. Rainfall simulators can be used on most dryland surfaces (aside from steep slopes), but require substantial volumes of water. The setup and experimentation times are also relatively long. Conversely, infiltrometers use relatively small water volumes per measurement and infiltrometer tests can be repeated, permitting improved sampling of spatial variability. However, the range of surface types is limited to flat, stone- and vegetation- free surfaces and some infiltrometers disturb surface crusts; as such their measured infiltration rates are not representative of drylands. Moreover, infiltrometers cannot be used to indicate, at least not directly, downslope transfer of water or establishment of surface hydrological connections to an outlet.

Considering overland flows, plot-scale studies can be set up using rainfall simulators (Dunkerley, 2012; Sharpley & Kleinman, 2003) though, as noted previously, these require considerable time to perform. Other overland flow tests use a trough overflowing at a constant (adjustable) rate (e.g. Abrahams & Parsons, 1991) which effectively applies water to the upslope width of a plot. Smith et al. (2011) also used a trough to provide constant discharge; however, in this example, runoff was not confined to a plot lower boundary enabling the wetting front to be tracked until water could not travel further. The method is further enhanced by capturing the microtopography of the channel using a terrestrial laser scanner facilitating approximate estimation of flow depths. Yet, the application of water to the surface from an overland flow trough can result in friction factors up to an order of magnitude lower than those observed during rainfall simulations (Parsons, Abrahams, & Wainwright, 1994). Li (2009) explored potential reasons for such differences, identifying complex interactions between different sources of flow resistance (e.g. grain, form, rainfall). The traditional linear superposition assumption (i.e. that the composite resistance of different roughness types is equal to the sum of individual resistance) was observed to be invalid, highlighting the complexity of surface runoff during natural rain events.

There is a clear need for a new measurement technique to better represent the hydrological response of dryland surfaces that combines the logistical advantages of infiltrometers with the process representation of rainfall simulators, and that can be used on the entire range of dryland surfaces. Here, we present a new approach to measuring surface hydrological response that aggregates the combined effect of infiltration and surface runoff transmission whilst providing a meaningful representation of the potential of a location to develop surface hydrological connections to stream networks and thereby contribute to flood flows.

3. Methods and Field Site

3.1 A new connectivity-based measurement of surface hydrological response

The propensity of a surface to convey water downslope, thereby overcoming both infiltration losses and overland flow resistance, can be measured in the field by dosing the surface with a set volume of water and tracking its passage downslope. The response of the surface can be quantified by mapping the downslope advance of the applied water over time (Figure 2). We developed an affordable and reproducible system of making these quick, easy and hydrologically-meaningful field measurements that can be readily coupled with Structure from Motion (SfM) photogrammetry to yield information about the surface properties, alongside the hydrological response.

Our dosing system comprised a 40 cm long horticultural planting trough with a capacity of 6 L which was used as a reservoir (Figure 2) and fixed to a housing constructed from oriented strand board (OSB) due to its tensile strength, low weight and low cost. The long axis of the trough was positioned perpendicular to the steepest angle of slope. A second, identical trough could be inserted and pushed into the reservoir trough held in the OSB housing, to produce a constant discharge (here 0.25 L s^{-1}) from the reservoir for a set duration (10 s). This flow rate yields runoff depths that match those recorded during storm events at the field site (section 3.3) on nearby hillslope crest stage gauges and is commensurate with runoff rates applied for measurements on similar semi-arid surfaces (e.g. Smith et al., 2011). While it is acknowledged that appropriate application rates would vary with hillslope position, application rates are necessarily standardised here to enable comparison of surfaces. A 37.5 cm slit cut into the reservoir trough allowed water to flow evenly out onto the ground. Evenly-distributed flow was ensured by a thin aluminium sheet bent to a 45˚ angle, which was attached below the slit. To ensure the inflow boundary remained horizontal on almost any surface, thereby ensuring even flow application rates, two orthogonally-oriented spirit levels and three flexible tripods were attached to the device.

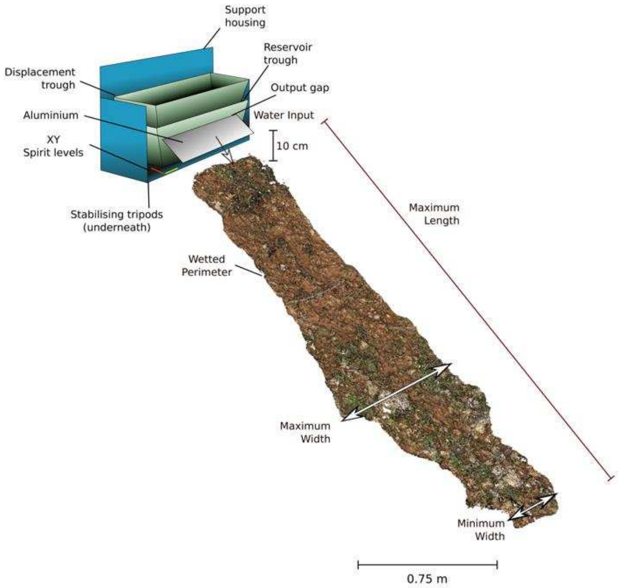

Figure 2. The field displacement trough manufactured for this study and illustration of hydrological measurements. Example dense point cloud with points coloured by RBG values also shown.

The flow rate can be adjusted by either increasing or decreasing the lowering rate of the displacement trough. Testing demonstrated that the application of 3 L of water over 10 s resulted in a relatively even distribution of water across the aluminium sheet. Over five test runs, water volumes measured in four collectors spread across the aluminium sheet were observed to vary by ±5 ml indicating a variability of just 1.5% of the total applied flow.

Water applied to the hillslope surface is allowed to move naturally through the landscape. The measurement is concluded when no further downslope advance of the water is observed; the interval between the initial water application and end of the measurement is timed and recorded (T_{max}, s). The overall geometry of the wetted area is captured both by measuring the main dimensions with a tape measure in the field (Figure 2) and later via measurements from SfM-derived orthophotographs. The maximum surface runoff length (L_{max}, m) and both maximum and minimum flow widths (W_{max}, W_{min}, m) are recorded.

Overall, the device is low in weight and can be carried in one hand with relative ease. Water requirements depend on the chosen application volume and were 2.5 L in the trial reported in this paper. The device can also be dismantled and reassembled for transportation making it highly portable. Field measurements took ~10-15 minutes and the total cost of the device was approximately £50.

3.2 Surface Properties

A suite of additional measurements taken in the field can be used to help explain variations in T_{max}, L_{max}, W_{max}, and W_{min}. These include variables measured rapidly in the field, and those calculated from subsequent post-processing (SfM photogrammetry).

Prior to each test a short field description of the study slope was made. The overall slope gradient and aspect were measured using a compass clinometer. Grain size distribution of the soil was identified using a hand lens and recorded according to the phi grain size classification (Wentworth, 1922). Following the application of water, the perimeter of the wetted area was outlined using brightly coloured chord. Multiple images of the wetted area were captured following standard and well-established SfM workflows (see Carrivick, Smith, & Quincey, 2016; Eltner et al., 2017 and Smith, Carrivick, & Quincey, 2016 for detailed descriptions). Multiple high-resolution images (mean 65, minimum 23 and maximum 168 based on the dimensions of the wetted area) were captured using a handheld Canon 60D (18MP resolution) DSLR camera with a Canon EF 28-135 mm *f*/3.5-5.6 mm lens. Images were captured at a 28 mm focal length, which was used for all of the measurements. Normally, due to the wide focal length this would result in lens distortion; however, as the Canon 60D has a 1.6x APS-C crop sensor, lens distortion is mitigated when using an EF mounted lens (O'Connor, Smith, & James, 2017) as well as automatic correction as part of the SfM workflow. The crop sensor results in an effective focal length of 44.8 mm (O'Connor et al., 2017). Images were captured from different perspectives surrounding the wetted area to minimise occlusions. SfM processing was performed using Agisoft PhotoScan v1.4.2 (Agisoft, 2018).

The advantages of SfM over other high-resolution survey techniques are well documented (e.g. Carrivick et al., 2016; Chandler & Buckley, 2016; Westoby, Brasington, Glasser, Hambrey, & Reynolds, 2012). Specifically for this application, SfM is ideal as it is quick, non-contact and provides dense topographic information accurate to mm-scale when surveyed over a short range (~2 m) (Smith & Vericat, 2015). Moreover, it requires no additional bulky field equipment. However, further measurements are required to provide a scale and orientation to the resulting point cloud. Here, to reduce survey time we did not use a total station or differential GPS to survey ground control points as typically used for SfM workflows (Smith et al., 2016). Instead, we used standard adjustable 5 m measuring staffs placed alongside the wetted area to provide reference scale bars and enable the point cloud to be scaled in a local coordinate system. All axes were scaled simultaneously using staffs placed on sloped surfaces. Vertical height between the flow start and finish points was calculated and compared to the height of the 3D point cloud to check that the model was correctly scaled. This setup resulted in an average georeferencing error of 0.013 m.

A scaled dense point cloud was generated in Agisoft PhotoScan which contained between ~2.7×10^6 and ~1.2×10^7 points. Dense clouds were exported to CloudCompare (CloudCompare, 2018). The dense cloud was linearly detrended and cropped to just the wetted area. To reduce processing time, while eliminating any potential point clusters and ensuring a more evenly sampled surface for unbiased roughness analysis (Smith & Warburton, 2018), level ten octree subsampling of the cloud was performed (~ 5 mm 3D point spacing). Vegetated areas were then manually edited out of the point cloud. CloudCompare was used to calculate surface roughness, defined as the median distance of points to a plane fitted to its nearest neighbours within a 50 mm radius, chosen to encompass any larger rock fragments.

In addition, for each test a 0.31 mm pixel resolution orthorectified mosaic image was generated perpendicular to the surface slope and exported as a .geotiff file to ArcMap (10.4). Each wetted outline was digitised manually, alongside areas covered by vegetation and stones. Field notes, the 3D model, and individual images used for SfM were used to identify the relationship of stones with the soil surface (i.e. surface or embedded) as it is thought to alter their hydrological influence (Poesen & Lavee, 1994). The total areas of each classification were then merged and measured and the area of vegetation, surface stones and embedded stones calculated as the percentage of total wetted area. Each of the three classes was calculated independently of the others, because vegetation can cover stones resting on the surface, and embedded stones can be covered by other stones (Figure 3).

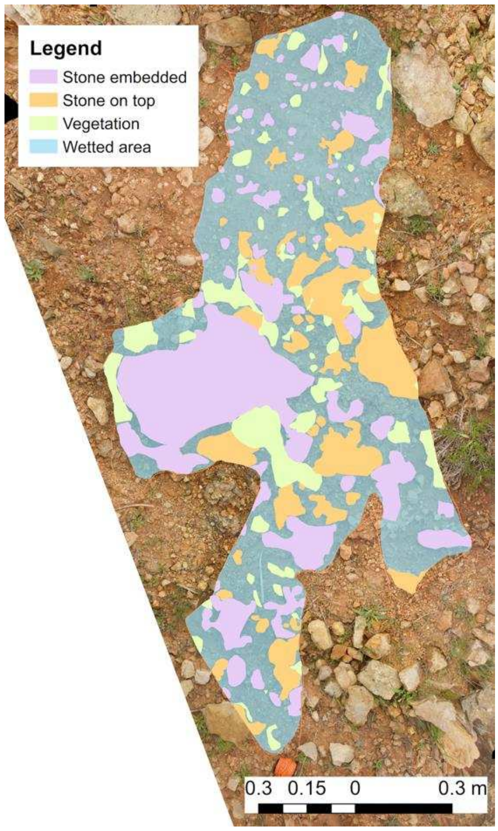

Figure 3. Example classified orthophoto mosaic (Location 1).

3.3 Field Site

The new method was tested on dryland hillslopes in south-west Portugal. A total of 64 tests of the new method were conducted across five locations chosen because they had a wide range of surface characteristics (Figure 4 and Table 1). Fieldwork was conducted over six days (23/03/18 – 28/03/18). The field sites that were used are located in the area around the coastal village of Salema, within the municipality of Vila do Bispo (Algarve region) (Figure 4). Average monthly temperatures in the area peak at 25°C in July, with lows of 12°C in January. Daily temperature fluctuations are more pronounced in comparison to the monthly averages (NOAA, 2018). Rainfall data collected in nearby Sagres (12 km from the field sites) since 1973 indicate that annual rainfall is highly variable and has averaged 479 mm; however, some years experienced double the average precipitation. This places the environment at risk for high intensity flooding and land degradation if not appropriately managed.

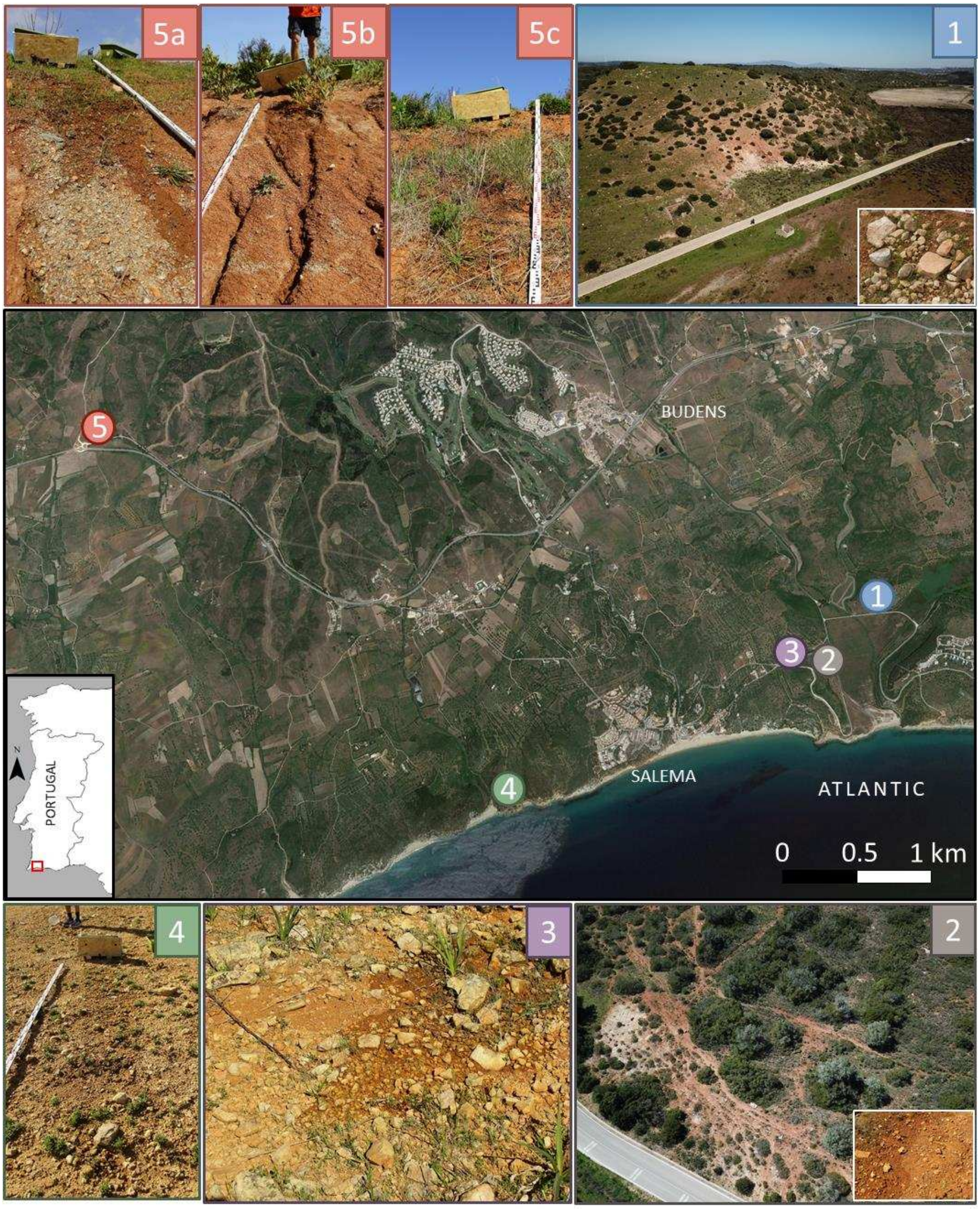

Figure 4. Aerial image of study area indicating test locations, as described in Table 1, including images of each experimental location. Aerial image: Google Earth: Terra Metrics 2019.

Location	Number of Tests	Mean Gradient (˚)	Mean Aspect	Vegetation Cover (%)	Embedded Stones (%)	Surface Stones	Mean Roughness

			(°)			(%)	(m x10^{-3})
1	19	24	181	14	14	12	4.76
2	8	20	123	10	26	19	3.67
3	5	22	128	35	8	11	4.14
4	7	11	123	9	49	20	3.01
5	25	28	208	18	1	0.2	4.15
5a	10	34	182	21	16	0.8	4.59
5b	11	20	257	10	1.5	0.4	3.40
5c	4	35	145	36	0.35	0	5.47

Table 1. Average descriptive characteristics for test locations. Note that site 5 is split owing to distinct slope differences within the site.

Details of the sites are given in Table 1. Test slopes were located in areas where surface characteristics were uniform along the length of the slope under investigation and where no artificial obstacles impeded water flow. The majority of slopes had a southerly aspect. Sites 1, 2 and 3 were located in the Boca do Rio valley; both sites 1 and 2 had a relatively low vegetation cover with a moderate (approximately 50%) stone cover. However, owing to the relatively large clast size, surface roughness was highest here. Site 3 had a higher vegetation cover with less pronounced surface stone cover. Site 4 was a shallow-gradient slope close to and facing the coastline with very low vegetation cover and a high stone coverage. Site 5 was notably different from all other sites being an artificially-graded slope close to a road with relatively steep gradients and low stone cover. Within site 5, three distinct slope units were used for measurements which had different combinations of slope and vegetation cover. Incised rills were pronounced at this site with clear evidence of flow concentration and recent sediment transport, though otherwise, surface roughness was minimal. Antecedent soil moisture was uniformly low owing to consistently dry weather conditions throughout the study period.

3.4 Statistical Analysis

Stepwise multiple linear regression was used to investigate relationships between each of the flow metrics (T_{max}, L_{max}, W_{max}, and W_{min}) and all measured surface properties. Using statistical functions in MATLAB 2018b, all variables in Table 1 were used in the initial linear model to assess their individual significance. Variables which were insignificant ($p > 0.1$) were removed from the model. Regression models were assessed for linearity, homoscedasticity, independence and normality to ensure statistical assumptions were met; raw residual (observed minus fitted values) outliers were removed where assumptions were not met.

4. Results

A wide range of hydrological responses was observed across the field site, despite identical rates of application of identical volumes of water (Figure 5). The differences between tests are easily visualised (see Figure 6 for examples) and a rich dataset of topography and imagery was available for further interrogation. Across the 64 tests, L_{max} varied between 1.08 and 6.55 m, W_{min} and W_{max} ranged between 0.01 and 0.38 m, and 0.42 and 1.05 m, respectively, whilst T_{max} varied between 18 and 103 s. Despite having moderately steep slopes, the lowest L_{max} values were observed at Site 3 (Figure 5A), where surface runoff typically remained diffuse and did not concentrate into narrow flow threads, reflected in the typically high W_{min} values (Figure 5C). Site 1 also exhibited diffuse flows; however, L_{max} values were higher at this site. Notably, distinct flow concentrations at Site 5 (e.g. Figure 6C-D) resulted in high L_{max} values, rapid runoff (low T_{max}) and low flow widths. Sites 2 and

4 responded relatively similarly to each other with intermediate values of many flow variables, though differences in T_{max} reflect the steeper slope at Site 2.

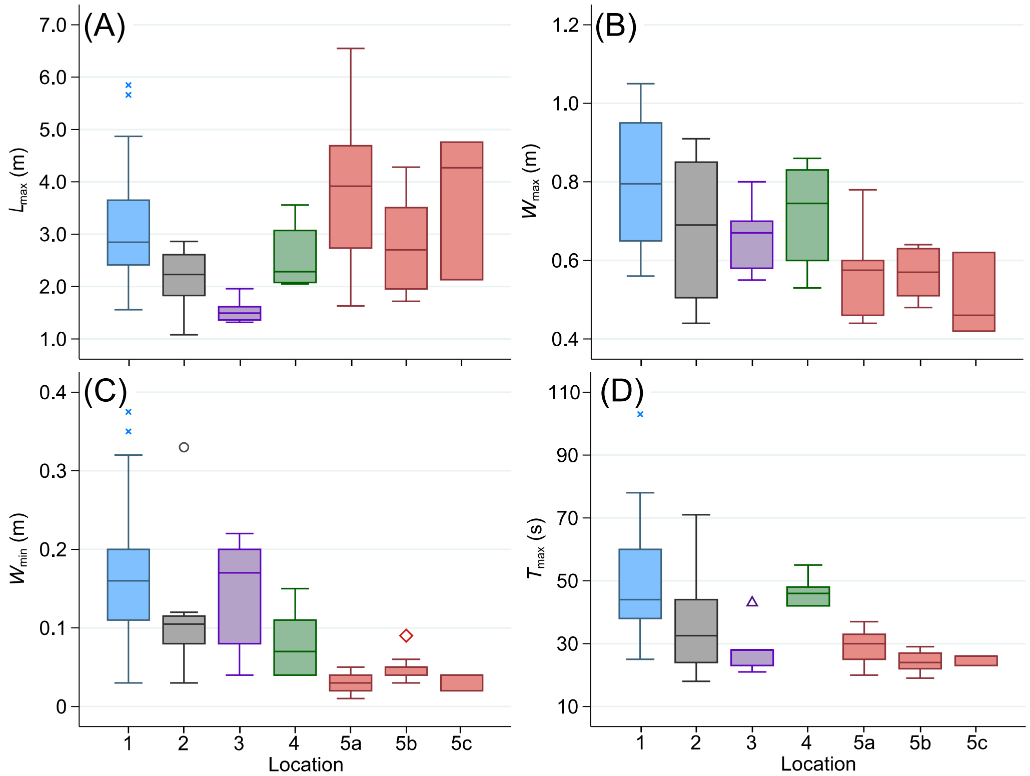

Figure 5. Box plots of flow metrics per location. Boxes show upper quartiles, medians and lower quartiles; whiskers extend to cover all points within 1.5 times the interquartile range of the quartiles; other points are shown separately.

Figure 6 shows classified orthophotographs from different locations in the field area. Runoff on the surfaces shown in Figures 6A and 6B is dispersed without much variation in width throughout the entire length, indicating more lateral connectivity; yet, as reflected in the L_{max}, weaker downslope connectivity. In contrast, the surfaces shown in Figures 6C and 6D both exhibit similar flow widths until flows become concentrated by the microtopography at approximately half of their total length, suggesting a relatively higher downslope connectivity than Figures 6A and 6B. Locations with less surface cover (e.g. location 5) have on average a higher L_{max} with lower W_{max} and W_{min} (see Figure 5), whereas locations with more surface cover have larger W_{max} and W_{min} with lower L_{max}. Multiple flow threads are also shown in Figure 6C and are representative of experiments at that location (80% of tests at location 5 generated multiple flow threads).

The multiple regression analysis revealed significant relationships between surface properties and each flow variable (Table 2). L_{max} is significantly ($p < 0.05$) influenced by vegetation cover and surface stone cover, with both exhibiting negative relationships (Table 2). Raw residuals greater than 2 m were removed ensuring normality and eliminating outliers. Embedded stones ($p = 0.162$) did not have a statistically significant impact on the maximum surface runoff length. Roughness and surface slope positively influenced L_{max}. The final multiple linear regression model ($p = < 0.001$, $R^2 = 0.403$, $df = 53$) is presented in Table 2 and Figure 7A.

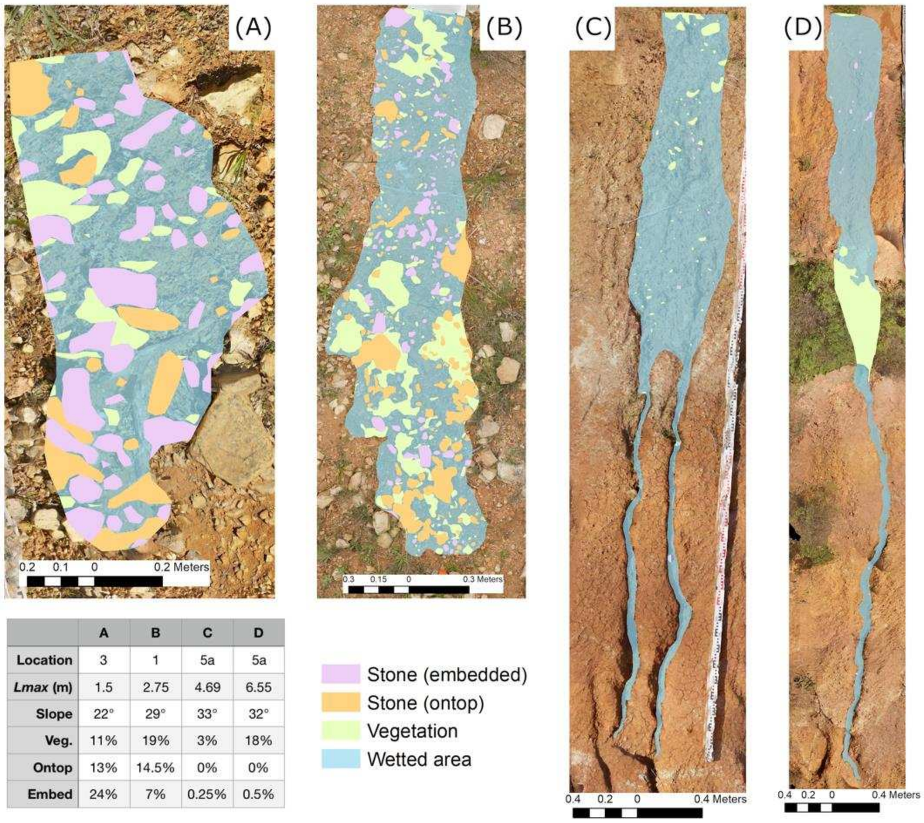

Figure 6. Sample of classified orthophotographs. Note the different scales.

	Coefficient	Standard error	*t*Stat	*p*-value
L_{max} (m) (Figure 7A)				
Vegetation(x_1)	-3.8732	0.8488	-4.5631	< 0.001
Surface Stones (x_2)	-1.799	0.7611	-2.3636	0.0218
Roughness (x_3)	308.05	133.42	2.3088	0.0249
Slope (x_4)	0.0433	0.0190	2.2801	0.0267
Intercept	1.2973	0.4956	2.6178	0.0115
W_{max} (m) (Figure 7B)				
Surface Stones (x_1)	0.4283	0.0933	4.5898	< 0.001
Embedded Stones (x_2)	0.1607	0.0664	2.4222	< 0.001
Intercept	0.5715	0.0192	29.738	0.0189
W_{min} (m) (Figure 7C)				
Roughness (x_1)	15.117	6.9616	2.1716	0.0345
Slope (x_2)	-0.0027	0.0010	-2.5563	0.0135
Upper Particle Size (x_3)	-0.0138	0.0037	-3.7479	< 0.001
Intercept	0.0205	0.0277	0.7384	0.4636
T_{max} (m) (Figure 7D)				
Surface Stones (x_1)	30.597	6.9467	4.4045	< 0.001
Embedded Stones (x_2)	20.685	4.9189	4.2053	< 0.001
Intercept	27.088	1.4362	18.861	< 0.001

Table 2. Linear regression model coefficients and significance for all flow variables. Model fits are visualised in Figure 7A-D.

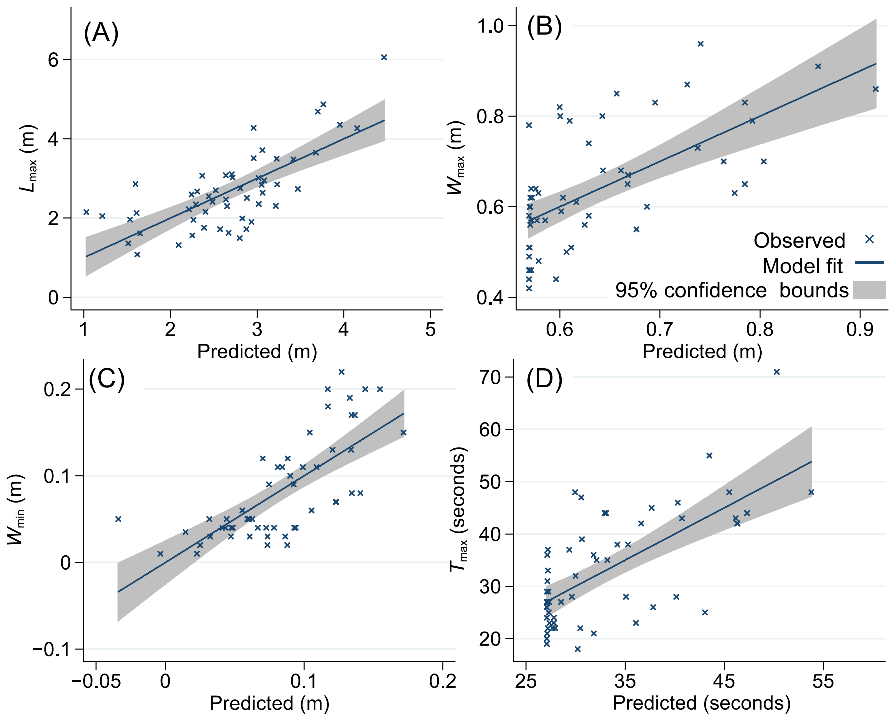

Figure 7. Performance of surface variable based multiple linear regression model predictions. See Table 2 and main text for details and performance of regression models.

W_{max} is also significantly (p < 0.05) controlled by surface cover. Specifically, surface stones and embedded stones exhibit a positive relationship with maximum width. Vegetation is statistically insignificant (p = 0.142) in terms of maximum width. Regression diagnostics resulted in raw residuals greater than 0.2 m being removed to ensure normality and remove outliers. The final multiple linear regression model (p = < 0.001, R^2 = 0.366, df = 53) is presented in Table 2 and Figure 7B.

W_{min} is significantly (p < 0.05) controlled by surface roughness, slope angle and particle size. Eight observations were removed due to raw residuals being greater than 0.1 m, thereby ensuring regression assumptions were met. The final multiple linear regression model (p = < 0.001, R^2 = 0.402, df = 52) is presented in Table 2 and Figure 7C. Increasing roughness and upper particle size both increase W_{min} (note that particle size increases as the phi class becomes more negative, resulting in the negative coefficient in Table 2). Increasing slope angle resulted in a decrease in W_{min}.

T_{max} showed a positive relationship with both surface and embedded stone cover (Figure 7D). Vegetation cover is not included in the final model as it was statistically insignificant (p = 0.541). Regression diagnostics resulted in outliers with raw residuals greater than 20 seconds (five tests) being removed to ensure normality. The final multiple linear regression model (p = < 0.001, R^2 = 0.45, df = 53) is presented in Table 2 and Figure 7D.

5. Discussion

5.1. Interpretation of runoff metrics

Representing the runoff response of dryland surfaces via the use of standardised surface flows is fundamentally different from conventional methods that typically focus on point measurements of infiltration. We have shown that the aggregation of infiltration and surface runoff dynamics into measurements of runoff dimensions is readily applicable to a range of dryland surfaces. However, the physical meaning of these measurements requires some consideration.

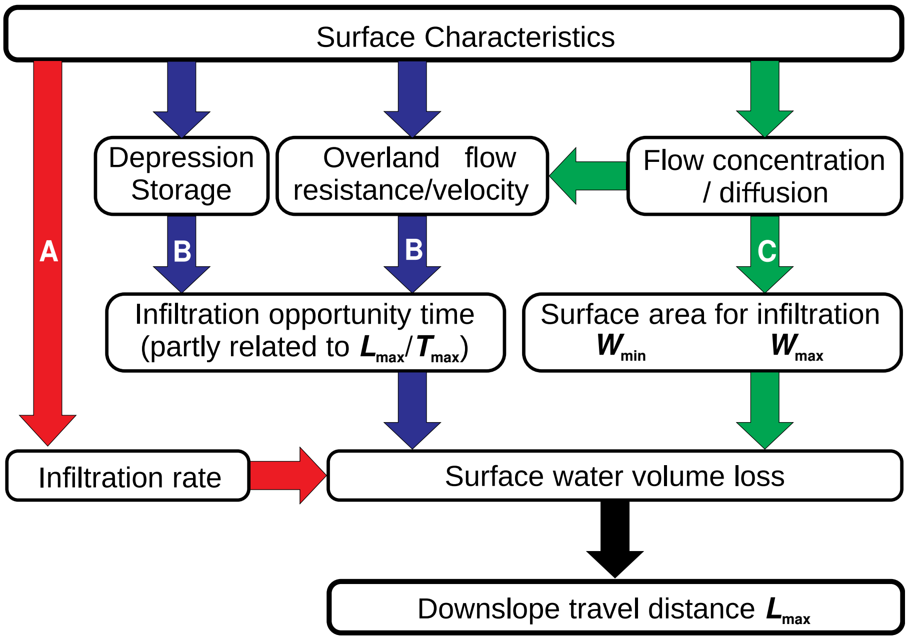

Figure 8. Conceptual summary of the relationships between surface characteristics and flow metrics measured in this study. Labels (A)-(C) indicate the three factors controlling infiltration volumes during the tests: (A) infiltration rate; (B) the time available for infiltration; and (C) surface area.

Within a hydrological connectivity framework, the primary variable of interest is L_{max} which represents the propensity of a surface to develop surface hydrological connections and transmit water downslope. During the timescale of field measurement whereby evaporation effects can be ignored, L_{max} is primarily limited by surface infiltration as the volume of water present on the surface is reduced gradually until no water remains to move downslope under gravity. The total water volume lost to infiltration is itself controlled by three main factors: (a) the infiltration rate; (b) the time available for infiltration as determined by the overland flow velocity; and (c) the area over which the water is spread as determined by local flow paths acting to concentrate or diffuse the flow (Figure 8). Thus, L_{max} measures more than just at-a-point infiltration; it also captures the dynamic relationship between infiltration loss and the hydraulics of overland flow. While L_{max} presently represents somewhat undefined combinations of the factors listed above, as a metric it is more directly correlated with connectivity than point measurements of infiltration, which rarely provide meaningful representations of functional connectivity, especially in drylands.

The additional metrics measured here provide some information as to the controls on L_{max}. The flow width metrics (W_{max} and W_{min}) provide greater insight into the surface area available for infiltration and how surface characteristics control the spread of flow laterally. T_{max} is related to the 'infiltration opportunity time' within the field measurements, and when scaled by the total distance travelled (i.e. L_{max} /T_{max}), it summarises the downslope velocity of the advancing water front. Overland flow resistance reduces the flow velocity and gives greater opportunity for water loss to the soil, potentially reducing L_{max}. Furthermore, some surface water may even become stored in depressions and prevented from further downslope travel.

5.2. Relationships with surface properties

Our trial of the new method clearly highlights its potential for identifying the main surface controls on runoff response. These are summarised in Figure 9.

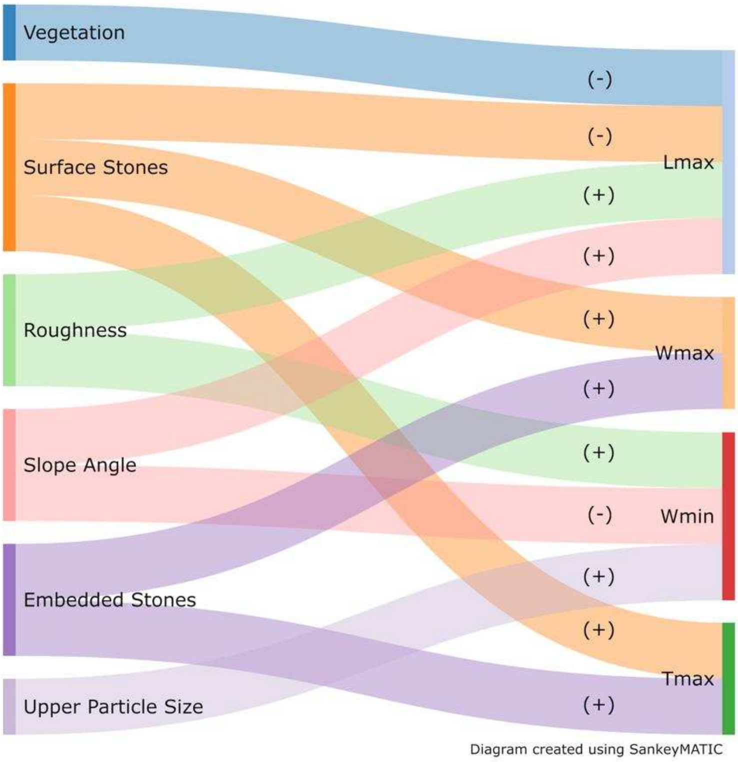

Figure 9. Summary of statistically significant ($p < 0.05$) relationships identified between surface runoff dimensions and surface conditions. Positive and negative relationships identified using (+) and (-) respectively.

L_{max} is positively related to slope angle and negatively related to vegetation cover. The slope effect is to be expected; increasing the gradient increases flow velocity, reduces the opportunity time for infiltration and leads to a greater L_{max} before all the water volume has infiltrated. The negative vegetation cover effect is most probably via enhanced infiltration under the vegetation canopy (Peng, Zhanbin, & Kexin, 2004). Surface stone cover is also observed to decrease L_{max}, possibly via such stones protecting underlying soil from sealing (Poesen, 1986) or via a flow resistance effect (Abrahams, Parsons, & Luk, 1986). Interestingly, no such relationship was observed for embedded stones, emphasising the importance of position of the rocks relative to the soil surface in determining their hydrological influence (Poesen & Lavee, 1994). Finally, the positive relationship between L_{max} and surface roughness indicates that localised roughness elements act to concentrate flow instead of providing local barriers and encouraging surface ponding as expected from roughness elements arranged parallel to the contours (Kirkby, 2001; Smith et al., 2011). Field observations (Figures 4 and 6) confirm this suggestion, where more concentrated and erosive flow threads reduce the flow width and hence reduce the total wetted area and decrease total infiltration during a test.

The regression analysis indicated that W_{max} was controlled by the presence of stone cover, with increasing concentrations of both surface and embedded stones, increasing W_{max}. The permeability of stones can be expected to be much lower than that of soil (Bear, 1972) causing a reduction in local infiltration, leaving a greater volume of water to be dispersed on the soil surface. Our evaluation of imagery from the test sites also indicates that the stone cover forced flow around the stone itself, encouraging further lateral spreading. However, it should be noted that we included the entire surface of clasts that were not fully submerged in our analysis. There was insufficient field time to identify dry emergent areas that had no contact with the flowing water and it was difficult to discern them from the imagery with confidence. The addition of a dye into the simulated surface runoff may overcome this limitation in future and would facilitate supervised classification of orthomosaic imagery to identify wetted areas automatically. Notably, these same two controls (surface and embedded stone cover) were also positively related to T_{max}. Thus, in the action of spreading the surface runoff, the hydraulic resistance was also increased, and the wetted area progressed more slowly across the surface.

The minimum flow width W_{min} acts as an indicator of flow concentration. More concentrated flows were formed on steeper slopes and those with smaller particle sizes (i.e. less negative phi classes). The increasing potential for flows to erode concentrated channels on steeper slopes is well established, while smaller particle sizes minimise lateral flow spreading. W_{min} increased with increasing surface roughness. This positive relationship reflects the dual role of roughness elements: rougher surfaces were observed to both spread surface flows (as per Figure 6A-B) and to concentrate surface flows (as per Figure 6C-D) and highlights the need for further efforts to examine these competing effects further. Disentangling the complex effect of roughness on surface runoff has been the focus of much research (e.g. Kamphorst et al., 2000; Smith et al., 2011) and a basic indication of the multiple influences of roughness has been identified from our simple field tests. More detailed calculation of alternative roughness parameterisations (see Smith, 2014) that isolate either flow concentration or flow blocking effects of surface roughness would further develop this analysis.

5.3. Future potential and limitations of surface runoff based approach

The range of surfaces sampled using the new method (Figure 5) could not have been sampled by either rainfall simulation or infiltrometers. High slope angles would have hampered rainfall simulation, while high surface stone covers would hinder either the insertion of ring infiltrometers into the soil or the maintenance of an adequate surface contact for tension infiltrometers. While Minidisk infiltrometers could have sampled the inter-stone surfaces, this would not have adequately represented the observed surface conditions relevant to characterising surface runoff processes (i.e. they cannot be used on stone surfaces themselves). Notably, the wetted areas of the tests ranged from 0.37 to 7.12 m^2 thereby sampling a much greater surface area than a Minidisk (typically 15.9 cm^2 of surface contact based on a 4.5 cm diameter base; Decagon Devices, 2016).

The new method proved simple to use on slopes with varying levels of cover at steep angles; applying surface runoff to the surface was straightforward. The apparatus was easy to carry, and field users were able to perform up to 27 tests per day over sometimes challenging terrain. However, two operators were found to be necessary for the safe use of the method on steep terrain. While water consumption (2.5 L per test) is substantially greater than for Minidisk infiltrometers, it is also substantially less than for rainfall simulation.

The method presented here offers a new perspective on quantifying surface hydrological response that diverges markedly from conventional vertical infiltration based approaches. The significance of surface hydrological connections is most pronounced in areas of Hortonian runoff generation. While we designed the method for drylands, we recognise that it is applicable in a wider range of environments. Although it measures the aggregate effect of multiple surface processes (infiltration and overland flow hydraulics), the method provides information of more direct relevance to water resource and flood managers. Deployment of the method over a catchment has the potential to identify hillslopes vulnerable to flow concentration which can increase downslope surface hydrological connectivity and overall flood volumes. Implementing flood management strategies in key locations could disconnect overland flow and provide opportunities to develop water storage offline from the river potentially reducing flooding downstream, providing a targeted preparation strategy for flood managers in dryland environments.

It represents a move away from developing a reductionist understanding of the physics of infiltration and overland flow hydraulics and instead yields metrics of surface runoff response that are pragmatic, conceptually simple, and well-aligned with contemporary connectivity-focused understandings of dryland catchment hydrology. The proposed field method is perhaps best considered alongside modelled connectivity indices based on mapped flow path lengths (e.g. Mayor et al., 2008).

In common with all existing methods, there are limitations as to where this method can be applied. First, a sloping surface is required. Second, areas of very high vegetation cover are challenging to work in. Though surface runoff dimensions around dense vegetation can still be measured in the field, they would be subject to greater errors and it would not be possible to obtain supplementary information from concurrent SfM surveys. Third, the evaluation of surface connectivity in this way is limited to the plot or small hillslope scale.

Additionally, the simple runoff simulation outlined here does not fully represent all the relevant processes in a natural runoff event. While a constant and relatively high volume of flow is applied, both the water application rate and volume can be varied easily and provide further information on their effect on flow lengths. However, the proposed method does not simulate rainfall and thus cannot recreate rainfall effects on flow resistance or surface sealing from raindrop impact, although previous surface sealing will likely have an effect on the outcome of the tests. In addition, the new method does not damage the surface unlike all infiltrometer methods previously mentioned. The method is biased towards concentrated flows as there is not an even supply of water across all the surface as provided by rainfall simulation; localised topographic highs remain dry throughout as flow threads develop around them. Yet, despite these limitations, it does simulate a much wider range of surface processes than achieved via conventional techniques. Future work could couple our proposed approach with time-varying runoff application and unbounded rainfall simulation.

6. Conclusions

Current infiltration measurement methods are unsuitable for natural dryland surfaces that typically exhibit high stone contents and complex vegetation patterns. We present an alternative method of quantifying dryland surface runoff response. While this does not map directly onto infiltration measurement, it provides an arguably more meaningful aggregation of multiple surface hydrological processes. Rapid and easy field deployment permits a high number of test runs within a single field campaign allowing for a wide range of dryland surfaces to be sampled. The method yields data that are well aligned with the conceptualisation of surface runoff processes in terms of functional or ‘process-based’ connectivity and can yield information on the development of surface hydrological connections. The new method represents the propensity, in aggregate, of a surface to develop surface hydrological connections and transmit water downslope; this propensity is highly significant in terms of both water resource and flood management.

Data Availability Statement
The data that support the findings of this study are available from the corresponding author upon reasonable request.

References

Abrahams, A. D., Parsons, A. J, & S. -H. Luk. (1986). Resistance to overland flow on desert hillslopes. *Journal of Hydrology, 88*(3-4), pp.343-363.

Abrahams, A. D. & Parsons, A, J. (1991). Resistance to overland flow on desert pavements and its implications for sediment transport modelling. *Water Resources Research, 27*(8), pp.1827-1836.

Abrahams, A. D., Parsons, A. J., & Wainwright, J. (1995). Effects of vegetation change on interrill runoff and erosion, Walnut Gulch, southern Arizona. *Geomorphology, 13*, pp.37−48.

Abrahams, A. D., Li, G., Krishnan, C., & Atkinson, J. F. (1998). Predicting sediment transport by interrill overland flow on rough surfaces. *Earth Surface Processes Landforms*, *23*, pp.1087-1099.

AgiSoft PhotoScan Professional (Version 1.4.2) [Software]. 2018. Retrieved from http://www.agisoft.com/downloads/installer/

Al-Awadhi, J. M. (2013). A case assessment of the mechanisms involved in human-induced land degradation in north-eastern Kuwait. *Land Degradation & Development, 24*(1), pp.2-11.

Ali, G. A. & Roy, A. G. (2009). Revisiting hydrologic sampling strategies for an accurate assessment of hydrologic connectivity in humid temperate systems. *Geography Compass, 3*, pp.350–374.

Ambroise, B. (2004). Variable 'active' versus 'contributing' areas or periods: a necessary distinction. *Hydrological Processes, 18*, pp.1149−1155.

Amoozegar, A. & Wilson, G. V. (1999). Methods for measuring hydraulic conductivity and drainable porosity. *Agricultural drainage,* pp.1149-1205.

Ankeny, M., Kaspar, T. C., & Horton, R. (1988). Design for an automated tension infiltrometer. *Soil Science Society of America Journal, 52*(3), pp.893-896.

Arnau-Rosalen, E., Calvo-Cases, A., Boix-Fayos, C., Lavee, H., & Sarah, P. (2008). Analysis of soil surface component patterns affecting runoff generation. An example of methods applied to Mediterranean hillslopes in Alicante (Spain). *Geomorphology, 101*(4), pp.595-606.

Bear, J. (1972). *Dynamics of Fluids in Porous Media*. Dover Publications.

Bergkamp, G., Cerda A., & Imeson, A. C. (1999). Magnitude-frequency analysis of water redistribution along a climate gradient in Spain. *Catena, 37*(1-2), pp.129-146.

Bracken, L. J. & Croke, J. (2007). The concept of connectivity and its application in geomorphology. *Hydrological Processes, 21*, pp.1749−1763.

Bracken, L. J., Wainwright, J., Ali, G. A., Tetzlaff, D., Smith, M. W., Reaney, S. M., & Roy, A. G. (2013). Concepts of hydrological connectivity: Research approaches, pathways and future agendas. *Earth-Science Reviews, 119*, pp.17-34

Brady, N. & Weil, R. (2008). *The nature and properties of soils.* Harlow: Prentice Hall.

Carrivick, J. L., Smith M. W., & Quincey, D. J. (2016). *Structure from Motion in the Geosciences.* John Wiley & Sons.

Chandler, J. H. & Buckley, S. (2016). Structure from motion (SFM) photogrammetry vs terrestrial laser scanning. *In:* M. B. Carpenter and C. M. Keane, (Eds.). *Geoscience Handboook 2016: AGI Data Sheets.* (5th ed). Alexandria, VA: American Geosciences Institute, Section 20.1.

Chen, L., Sela, S., Svoray, T., & Assouline, S. (2013). The role of soil-surface sealing, microtopography, and vegetation patches in rainfall-runoff processes in semiarid areas. *Water Resources Research, 49*(9), pp.5585-5599.

CloudCompare (version 2.10.1) [GPL software]. (2016). Retrieved from: http:www.cloudcompare.org/

Decagon Devices. (2016). *Mini Disk Infiltrometer*. Pullman, WA.

Dimanche, P. H. & Hoogmoed, W. B. (2002). Soil tillage and water infiltration in semi-arid Morocco: the role of surface and sub-surface soil conditions. *Soil & Tillage Research*, *66*(1), pp.13-21.

Dunkerley, D. (2004). Flow threads in surface run-off: Implications for the assessment of flow properties and friction coefficients in soil erosion and hydraulics investigations. *Earth Surface Processes and Landforms*, *29*(8), pp.1011-1026.

Dunkerley, D. (2012). Effects of rainfall intensity fluctuations on infiltration and runoff: rainfall simulation on dryland soils, Fowlers Gap, Australia. *Hydrological Processes, 26*(15), pp.2211-2224.

Dunkerley, D. (2018). How is overland flow produced under intermittent rain? An analysis using plot-scale rainfall simulation on dryland soils. *Journal of Hydrology*, *556*, pp.119-130.

Eltner, A., Kaiser, A., Castillo, C., Rock, G., Neugirg, F., & Abellán, A., (2016). Image-based surface reconstruction in geomorphometry–merits, limits and developments. *Earth Surface Dynamics*, *4*(2), pp.359-389.

Fitzjohn, C., Ternan, J.L., & Williams, A.G. (1998). Soil moisture variability in a semi-arid gully catchment: Implications for runoff and erosion control. *Catena, 32*, pp.55−70.

Guzha, A. C. (2004). Effects of tillage on soil microrelief, surface depression storage and soil water storage. *Soil & Tillage Research, 76*(2), pp.105-114.

Heckmann, T., Cavalli, M., Cerdan, O., Foerster, S., Javaux, M., Lode, E., Smetanova, A., Vericat, D. & Brardinoni, F. (2018). Indices of sediment connectivity: opportunities, challenges and limitations. *Earth-Science Reviews*, 187, pp.77-108.

Heilweil, V. M., Mckinney, T. S., Zhdanov, M. S., & Watt D. E. (2007). Controls on the variability of net infiltration to desert sandstone. *Water Resources Research, 43*(7).

Hikel, H., Yair, A., Schwanghart, W., Hoffmann, U., Straehl, S., & Kuhn, N. J. (2013). Experimental investigation of soil ecohydrology on rocky desert slopes in the Negev Highlands, Israel. *Zeitschrift Fur Geomorphologie, 57*, pp.39-58.

Huang, J., Li, Y., Fu, C., Chen, F., Fu, Q., Dai, A.… & G. Wang. (2017). Dryland climate change: Recent progress and challenges. *Reviews of Geophysics, 55*(3), pp.719-778.

Kamphorst, E. C., Jetten, V., Guérif, J., Pitkänen, J., Iversen, B. V., Douglas, J.T., & Paz, A. (2000). Predicting depressional storage from soil surface roughness. *Soil Science Society of America Journal 64*, pp.1749−1758.

Keesstra, S., Nunes, J. P., Saco, P., Parsons, T., Poeppl, R., Masselink, R. & Cerdà, A. (2018). The way forward: Can connectivity be useful to design better measuring and modelling schemes for water and sediment dynamics? *Science of the Total Environment*, 644, pp.1557-1572.

Kelishadi, H., Mosaddeghi, M. R., Hajabbasi, M. A., & Ayoubi, S. (2014). Near-saturated soil hydraulic properties as influenced by land use management systems in Koohrang region of central Zagros, Iran. *Geoderma, 213*, pp.426-434.

Kirkby, M. J. (2001). Modelling the interactions between soil surface properties and water erosion. *Catena, 46*, pp.89−102.

Kirkby, M. J., Bracken, L. J., & Reaney, S. (2002). The influence of land use, soils, and topography on the delivery of hillslope runoff to channels in SE Spain. *Earth Surface Processes and Landforms, 27*, pp.1457−1473.

Lai, J. & Ren, L. (2007). Assessing the size dependency of measured hydraulic conductivity using double-ring infiltrometers and numerical simulation. *Soil Science Society of America Journal, 71*(6), pp.1667-1675.

Li, G. (2009). Preliminary study of the interference of surface objects and rainfall in overland flow resistance. *Catena, 78,* pp.154-158.

Li, X. Y., Gonzalez, A., & Sole-Benet, A. (2005). Laboratory methods for the estimation of infiltration rate of soil crusts in the Tabernas Desert badlands. *Catena, 60*(3), pp.255-266.

Martínez-Mena, M., Albaladejo, J., & Castillo, V. M. (1998). Factors influencing surface runoff generation in a Mediterranean semi-arid environment: Chicamo watershed, SE Spain. *Hydrological Processes, 12*, pp.741−754.

Mayor, Á. G., Bautista, S., Small, E. E., Dixon, M., & Bellot, J. (2008). Measurement of the connectivity of runoff source areas as determined by vegetation pattern and topography: A tool for assessing potential water and soil losses in drylands. *Water Resources Research*, *44*, pp.1-13.

Middleton, N. & Thomas, D. (1997). *World atlas of desertification.* (2nd ed). London: Arnold.

Mueller, E. N., Wainwright, J., & Parsons, A. (2007). Impact of connectivity on the modeling of overland flow within semiarid shrubland environments. *Water Resources Research, 43*, W09412, doi:10.1029/2006WR005006.

NOAA. (2018). Integrated Surface Database Station History, August 2018. [online]. [Accessed 05/08/2018]. Available from: https://www.ncdc.noaa.gov/.

O'Connor, J., Smith, M. J., & James, M. R. (2017). Cameras and settings for aerial surveys in the geosciences: optimising image data. *Progress in Physical Geography, 41*(3), pp.325-344.

Parsons, A. J., Abrahams, A. D., & Wainwright, J. (1994). On determining resistance to interrill overland flow. *Water Resources Research, 30*(12), pp.3515-3521.

Peng, L., Zhanbin, L., & Kexin, L. (2004). Effect of vegetation cover types on soil infiltration under simulating rainfall. *In: 13th International Soil Conservation Organisation Conference.*

Perrolf, K. & Sandstrom, K. (1995). Correlating landscape characteristics and infiltration - A study of surface sealing and subsoil conditions in semi-arid Botswana and Tanzania. *Geografiska Annaler Series a-Physical Geography, 77A*(3), pp.119-133.

Perroux, K. & White, I. (1988). Designs for disc permeameters. *Soil Science Society of America Journal, 52*(5), pp.1205-1215.

Pierson, F. B., Williams, C. J., Kormos, P. R., Hardegree, S. P., Clark, P. E., & Rau, B. M. (2010). Hydrologic Vulnerability of Sagebrush Steppe Following Pinyon and Juniper Encroachment. *Rangeland Ecology & Management, 63*(6), pp.614-629.

Poesen, J. (1986). Surface sealing as influenced by slope angle and position of simulated stones in the top layer of loose sediments. *Earth Surface Processes and Landforms, 11*(1), pp.1-10.

Poesen, J. & Lavee, H. (1994). Rock fragments in top soils: significance and processes. *Catena, 23*(1-2), pp.1-28.

Reaney, S. M., Bracken, L. J., & Kirkby, M. J. (2007). Use of the Connectivity of Runoff Model (CRUM) to investigate the influence of storm characteristics on runoff generation and connectivity in semi-arid areas. *Hydrological Processes, 21*, pp.894−906.

Reaney, S. M., Bracken, L. J., & Kirkby, M. J. (2014). The importance of surface controls on overland flow connectivity in semi-arid environments: Results from a numerical experimental approach. *Hydrological Processes, 28*(4), pp.2116-2128.

Reynolds, W. D., Elrick, D. E., Youngs, E. G., & Amoozegar, A. (2002). 3.4.3.1 Introduction. *In:* J. H. DANE and C. G. TOPP (Eds). *Methods of Soil Analysis: Part 4 Physical Methods.* Madison, WI: Soil Science Society of America, pp.817-843.

Safriel, D., Adeel, Z., Niemeijer, D., Puigdefabregas, J., White, R., Lal, R… & Mcnab D. (2005*). Dryland Systems*. *In:* El-Kassas, M. & Ezcurra, E. (Eds). *Millenium Ecosystem Assessment.*

Sanders, L. (1998). *A manual of field hydrogeology.* Upper Saddle River, N.J.

Schreiner-McGraw, A. P. & Vivoni, E. R. (2018). On the sensitivity of hillslope runoff and channel transmission losses in arid piedmont slopes. *Water Resources Research*, *54*(7), pp.4498-4518.

Seeger, M. (2007). Uncertainty of factors determining runoff and erosion processes as quantified by rainfall simulations. *Catena, 71*(1), pp.56-67.

Sharpley, A., & Kleinman, P. (2003). Effect of rainfall simulator and plot scale on overland flow and phosphorus transport. *Journal of environmental quality, 32*(6), pp.2172-2179.

Simonneaux, V., Cheggour, A., Deschamps, C., Mouillot, F., Cerdan, O., & Le Bissonnais, Y. (2015). Land use and climate change effects on soil erosion in a semi-arid mountainous watershed (High Atlas, Morocco). *Journal of Arid Environments*, *122*, pp.64-75.

Smith M. W. (2014). Roughness in the Earth Sciences. *Earth Science Reviews, 136*, pp.202–225.

Smith, M. W. & Vericat, D. (2015). From experimental plots to experimental landscapes: topography, erosion and deposition in sub-humid badlands from structure-from-motion photogrammetry. *Earth Surface Processes and Landforms, 40*(12), pp.1656-1671.

Smith, M.W. & Warburton, J. (2018). Microtopography of bare peat: a conceptual model and objective classification from high-resolution topographic survey data. *Earth Surface Processes and Landforms*, *43*(8), pp.1557-1574.

Smith, M. W., Bracken, L. J., & Cox, N. J. (2010). Toward a dynamic representation of hydrological connectivity at the hillslope scale in semiarid areas. *Water Resources Research*, *46*(12).

Smith, M. W., Cox, N. J., & Bracken, L. J. (2011). Terrestrial laser scanning soil surfaces: A field methodology to examine soil surface roughness and overland flow hydraulics. *Hydrological Processes*, *25*(6), pp.842-860.

Smith, M. W., Carrivick, J. L., & Quincey, D. J. (2016). Structure from motion photogrammetry in physical geography. *Progress in Physical Geography*, *40*(2), pp.247-275.

Turnbull, L., Wainwright, J., & Brazier, R. E. (2008). A conceptual framework for understanding semi-arid land degradation: ecohydrological interactions across multiple-space and time scales. *Ecohydrology, 1*, pp.23–34.

Verbist, K., Torfs, S., Cornelis, W. M., Oyarzun, R., Soto, G., & Gabriels, D. (2010). Comparison of single- and double-ring infiltrometer methods on stony soils. *Vadose Zone Journal, 9*(2), pp.462-475.

Verbist, K., Cornelis, W. M., Torfs, S., & Gabriels, D. (2013). Comparing methods to determine hydraulic conductivities on stony soils. *Soil Science Society of America Journal, 77*(1), pp.25-42.

Wainwright, J. & Bracken, L. J. (2011). Runoff generation, overland flow and erosion on hillslopes, *In*: Thomas, D.S.G. (Ed.), *Arid Zone Geomorphology*, (3rd ed). John Wiley and Sons, Chichester.

Wainwright, J., Parsons, A. J., & Abrahams, A. D. (2000). Plot-scale studies of vegetation, overland flow and erosion interactions: case studies from Arizona and New Mexico. *Hydrological Processes*, *14*, pp.2921–2943.

Wentworth, C. K. (1922). A scale of grade and class terms for clastic sediments. *The Journal of Geology, 30*(5), pp.377-392.

Westoby, M. J., Brasington, J., Glasser, N. F., Hambrey, M. J., & Reynolds, J. M. (2012). 'Structure-from-Motion' photogrammetry: A low-cost, effective tool for geoscience applications. *Geomorphology*, *179*, pp.300-314.

Williams, J. D., Wuest, S. B., Schillinger, W. F., & Gollany, H. T. (2006). Rotary subsoiling newly planted winter wheat fields to improve infiltration in frozen soil. *Soil & Tillage Research, 86*(2), pp.141-151.

Wolman, M. G. & Gerson, R. (1978). Relative scales of time and effectiveness of climate in watershed geomorphology. *Earth Surface Processes & Landforms, 3*, pp.189−208.

Wu, L. & Pan, L. (1997). A generalized solution to infiltration from single-ring infiltrometers by scaling. *Soil Science Society of America Journal*, *61*(5), pp.1318-1322.

Xu, X., Lewis, C., Liu, W., Albertson, J. D., & G. Kiely. (2012). Analysis of single-ring infiltrometer data for soil hydraulic properties estimation: Comparison of BEST and Wu methods. *Agricultural Water Management, 107*, pp.34-41.

Young, M. H., McDonald, E. V., Caldwell, T. G., Benner, S. G., & Meadows, D. G. (2004). Hydraulic properties of a desert soil chronosequence in the Mojave desert, USA. *Vadose Zone Journal, 3*(3), pp.956-963.

Zhou, J., Hu, B. X., Cheng, G. D., Wang, G. X., & Li, X. (2011). Development of a three-dimensional watershed modelling system for water cycle in the middle part of the Heihe rivershed, in the west of China. *Hydrological Processes, 25*(12), pp.1964-1978.